Journal of Nano Research
ISSN: 1661-9897, Vol. 58, pp 102-117
doi:10.4028/www.scientific.net/JNanoR.58.102

Submitted: 2019-01-30
Revised: 2019-04-18
Accepted: 2019-05-03
Online: 2019-06-19

Structure, Microsctructure and Magnetic Properties of Ternary $(Fe_{0.6}Al_{0.4})_{100-x}Si_x$ Nanostructured Powders: Effect of Si Addition

N. Boukherroub[1,a], M. Hemmous[2,b], A. Guittoum[2,c*], D. Martínez-Blanco[3,d], N. Souami[2,e], P. Gorria[4,f], J.A. Blanco[5,g]

[1]UR-MPE, M'hamed Bougara University, Boumerdes, 35000, Algeria

[2]Nuclear Research Centre of Algiers, 02 Bd Frantz Fanon, BP 399 Alger-Gare, Algiers, Algeria

[3]SCTs, University of Oviedo, EPM, 33600 Mieres, Spain.

[4]Department of Physics & IUTA, EPI, University of Oviedo 33203 Gijón, Spain.

[5]Department of Physics, University of Oviedo, Calvo Sotelo St., 33007 Oviedo, Spain.

[a]nadia.boukherroub@yahoo.fr, [b]messaoudph@gmail.com, [c]aguittoum@gmail.com, [d]martinezbdavid@uniovi.es, [e]souaminassim@yahoo.fr, [f]pgorria@uniovi.es, [g]jabr@uniovi.es
*Corresponding author: aguittoum@gmail.com

Keywords: Nanostructured FeAlSi powders, mechanical alloying, microstructure, morphology, hysteresis loops, Mössbauer spectroscopy.

Abstract. Nanostructured $(Fe_{0.6}Al_{0.4})_{100-x}Si_x$ powders with x= 0, 5, 10, 15 and 20 at.% were elaborated by means of mechanical alloying for a fixed milling time of 72 h. We have investigated the effect of silicon addition on the microstructure and magnetic properties of these ternary alloys. X-ray diffraction experiments reveal that these powders are single-phase disordered solid solutions with body centered cubic crystal structure. The lattice parameter diminishes almost linearly as the Si content increases. The mean crystallite size, <D(nm)>, is around three times smaller for the samples with higher amount of Si (≈ 10 nm) compared with that of the binary alloy (27 nm). Moreover, the volume fraction of grain boundaries (fgb) seems to be higher with increasing the Si content, as well as both dislocation density (ρ) and lattice microstrain (<ε>), that follow a linear trend. The SEM images show that the Si helps in refining the shape and size of the powder particles, leading to a nearly homogeneous small particle. The addition of Si strongly affects the value of the saturation magnetization, Ms, that falls nearly an order of magnitude for the sample with 20 at.% Si, while the coercivity remains almost unchanged. The Mössbauer spectra show the presence of a sextet (ferromagnetic phase) and a singlet or a doublet (non ferromagnetic phase), except for the sample corresponding to x = 10, where only one singlet is observed in the spectrum.

1. Introduction

Mechanical alloying (MA) technique is a powerful method for the elaboration of powdered nanostructured materials. The physical-chemical properties of the nanostructured powders depend on different parameters such us: type of milling device, ball to powder mass ratio, milling time, cycle of milling, ...) and hence a careful choice of these parameters is essential in order to optimize thematerials'properties [1]. During the MA process the initial elemental powders are repeatedly deformed, cold welded and fractured until reaching the equilibrium state which corresponds to a minimum value of the crystallite size [2]. In the case of nanostructured ferromagnetic materials, if the cristallite size decreases down to the nanometric scale a change in the magnetic properties is frequently observed, which has been well explained by the random anisotropy model (RAM) [3, 4]. Ternary nanocrystalline Fe-Al-X (X=Ni, Mn, Cu, Ti, Cr, B, Si) alloys elaborated by MA exhibit a nanostructured state that have been extensively investigated due to their interesting magnetic behaviour [5]. In addition, the MA technique induces different phase transformations in these metallic systems, even in out-of-equilibrium conditions [3]. A particular interest has been focused towards the nanocrystalline Fe-rich Fe-Al-Si alloys, especially $(Fe_{0.8}Al_{0.2})_{100-x}Si_x$ and $(Fe_{0.7}Al_{0.3})_{100-x}Si_x$fabricated under diverseconditions using different planetary mills [6-9]. The evolution of microstructural and

magnetic properties are directly related to the chemical composition of the particular alloy and to the elaboration conditions. However, the $Fe_{60}Al_{40}$ binary alloy displays a particular interest because its magnetic behavior (ferro- or paramagnetic) depends on the degree of disorder of the alloy [10, 11]. Then, the addition of a third element, such as silicon, and the use of MA as fabrication method, allow obtaining nanocrystalline disordered solid solutions in which we expect important changes of the magnetic behaviour. To the best of our knowledge, few works have been reported on the nanocrystalline ternary $(Fe_{0.6}Al_{0.4})_{100-x}Si_x$ alloys prepared by MA from elementary Fe, Al and Si powders. Hence, the curiosity on these ternary systems, and especially the effect that the addition of Si could have on the microstructure and consequently on the magnetic behavior, is the main motivation to undertake this research work.

2. Experimental Procedure

2. 1. Elaboration of samples

$(Fe_{0.6}Al_{0.4})_{100-x}Si_x$ nanostructred alloys (with x=0, 5, 10, 15 and 20 at.%) were elaborated by mechanical alloying of elemental powders Fe, Al and Si with a purity of 99.99% and mean particle size of ~100 μm. The MA process was performed under anargon atmosphere using a vario-planetary high-energy-ball mill (FritschP4) which permits the control of the rotation speed of the main disc (Ω) as well as that of the vials (ω) separately, and consequently the mode milling (shock or friction).We have selected the friction mode (Ω<ω) with rotation speed values Ω =250 rpm for the disc and ω=400 rpm for the vials. The powders were milled for a fixed time of 72 h, which corresponds to the optimum duration for the single-phase formation of the binary Fe(Al) and tenary Fe(Al, Si) solid solutions as previously confirmed [8, 9]. The ball to powder weight ratio was fixed to 15:1. In order to prevent an excessive increase of the temperature inside the vials during the milling process, each period of 30 min of milling was followed by a pause of 15 min.

2.2. Characterization methods

The powder morphology and the chemical composition were analyzed with a scanning electron microscope (SEM, Philips XL 30) equipped with an energy-dispersive X-ray spectroscopy (EDX) analyzer.

The X-ray diffraction patterns were collected in a Philips X'Pert Pro powder diffractometer using Cu Kα radiation (λ=1.5418 Å), in the 2θ range between 10° and 110° with a step of 0.02°. In order to fix the shift of zero angle, a silicon crystal was used as a standard sample. The full profile fitting of the XRD lines was performed by means of the X'Pert High-Score software [12]. The latter uses analytical functions approximating the pseudo-Voigt function which is a linear combination of a Lorentzian (L) and a Gaussian (G) function. The XRD data allows to determine the crystal structure and the values of the lattice parameters of the samples, and to estimate the values of the mean crystallite size, <D> (nm), together with of the lattice microstrain, <ε> (%), through the Williamson–Hall method [13]. This procedure is based on the line-broadening of the Bragg reflections and is given by the following equation:

$$\beta \cos\theta = \frac{K\lambda}{D} + 2\varepsilon \sin\theta \quad (1)$$

where K is the Scherer constant, λ the wavelength of x-ray radiation, D the crystallite size, ε the lattice microstrain and θ is the Bragg angle. The parameter β is the full width at half-maximum of the Bragg peak (in fact, $\beta=\beta_{exp}-\beta_{inst}$, where β_{exp} is the measured width and β_{inst} is the instrumental width determined from the XRD pattern of a Si standard powder). The slope of the Williamson-Hall plot, βcos θ vs.2sinθ, gives us the value of the lattice microstrain, ε, and the intercept with the βcosθ axis gives the term Kλ/D, and then the value of the mean crystallite size. If we assume that a crystallite is a sphere of diameter D surrounded by a shell of grain boundary with thickness t, the volume fraction of grain boundary, f_{gb}, can be written as [14, 15]:

$$f_{gb} = 1 - f_g \quad (2)$$

where f_g is the volume fraction of the grains and is given by:

$$f_g = \frac{(D-t)^3}{D^3} \quad (3)$$

The values of f_{gb}, of $(Fe_{0.6}Al_{0.4})_{100-x}Si_x$ samples, were obtained from this equation taking into account the calculated values of D and assuming t = 1 nm.

The magnetization vs. applied magnetic field curves, M(H), were collected at room temperature with a LakeShore 7400 vibrating sample magnetometer (VSM), within the applied magnetic field range of ±7 kOe. The values of the saturation magnetization and coercivity for all the powder samples were estimated from the M(H) loops.

The Mössbauer spectra were collected at room temperature in transmission geometry with a constant-acceleration Wissel spectrometer, using a radioactive ^{57}Co-Rh source. The spectra were fitted with the Recoil software using the voigt-based hyperfine field distribution method (HFD-VB-F) [16]. The isomeric shift value was estimated taking that of α-Fe at 300 K as a reference value. From the fit of the spectra, we obtained the average hyperfine magnetic field <Hhf> wich is calculated using the following expression:

$$< H_{hf} >= \sum_i P_i\,(H_i) H_i \quad (4)$$

Were H_i is the magnetic field value of the i^{th} site and $P_i(H_i)$ is the calculated probability associated with the magnetic field H_i.

3. Results and Discussion

3.1. Morphological changes and chemical composition

Fig. 1 shows the change of the powder particle shape and size of $(Fe_{0.6}Al_{0.4})_{100-x}Si_x$ samples after 72 h of milling. The binary $Fe_{60}Al_{40}$ powder consists of large agglomerates with irregular shape and size. This could be due to the fact that both iron and aluminium are ductile, and therefore gives rise to the formation of alloy with a softer character that favours the coalescence between particles. These agglomerates become smaller as more silicon atoms are introduced into the powders, and their shape becomes gradually rounded. The latter suggests that the Si acts as a coalescence inhibitor and helps in the refining of the particle shape, leading to a nearly homogeneous small particle. A similar observation was already reported for nanostructured Fe-Co-Si and Fe-Al-Si alloys [8, 17, 21] and has been attributed to the fact that silicon is a brittle material and its introduction into a ductile iron lattice gives rise to harder compounds with more tendency to particle fragmentation as the amount of Si increases.

Energy dispersive X-ray analyses (EDX) were made on the samples. In Fig. 2 we present examples of EDX spectra corresponding to samples with lowest and highest Si content. We have noted that only the peaks belonging to Fe, Al and Si are present; hence, contamination from the vials and/or balls, during the milling process, is negligible within the experimental uncertainty of the EDX equipment. For the quantification, we have performed standardless ZAF simulation of EDX spectra (see Fig. 2) and we found that, for all samples, the composition is very close to the nominal one.

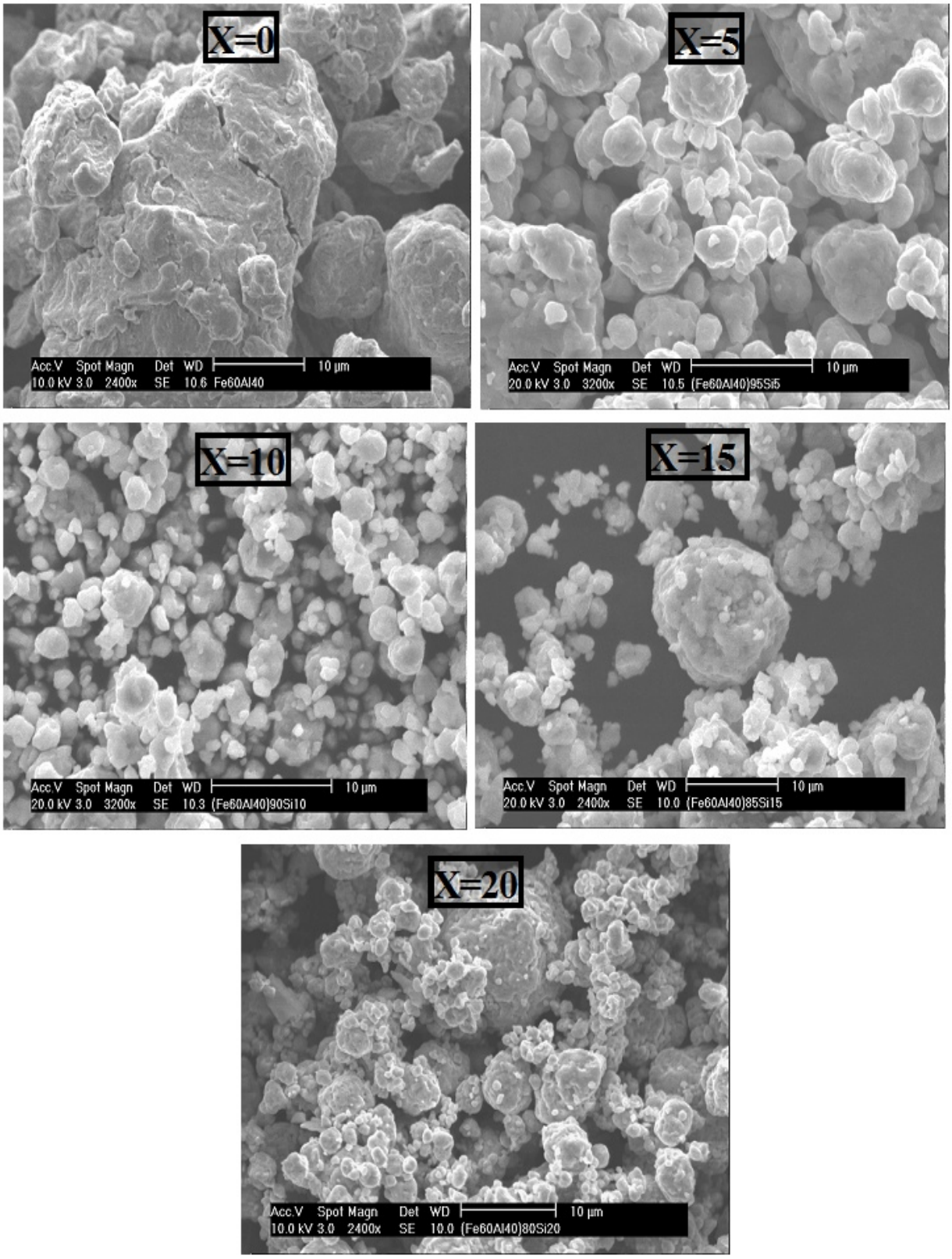

Figure 1. SEM images of $(Fe_{0.6}Al_{0.4})_{100-x}Si_x$ milled powders.

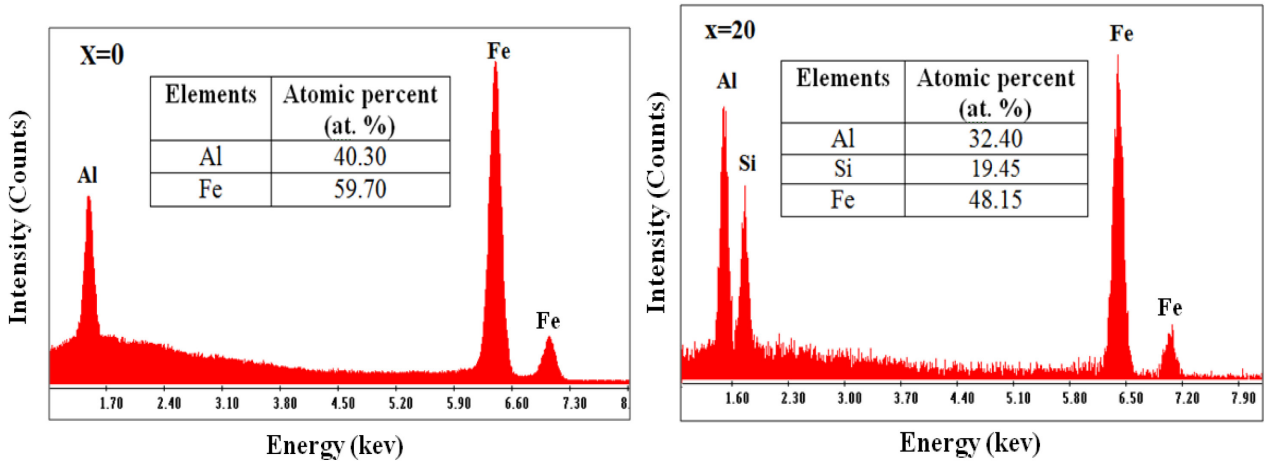

Figure 2. Examples of Energy dispersive X-ray (EDX) spectra for the samples with (a) x=0, and (b) x= 20.

3.2. X-ray diffraction and microstructural changes

The XRD patterns of $(Fe_{0.6}Al_{0.4})_{100-x}Si_x$ milled powders are shown in Fig. 3a, where the X-ray pattern of the Fe-Al-Si un-milled powders (0 h) is also shown for comparison. For 0 h of milling, the XRD pattern shows the peaks corresponding to iron (body centred cubic crystal structure, bcc) [18] and those of aluminium and silicon (face centered cubic crystal structure, fcc) [19, 20]. After 72 h of milling, all the observed peaks in the five diffraction patterns can be indexed as the Bragg reflections corresponding to a single phase with bcc crystal structure. It is worth noting the absence of any superstructure peak or any additional peaks coming from impurity phases and/or from pure Fe, Al or Si phases. This indicates that both Al and Si atoms diffused and randomly occupy some of the Fe sites within the conventional α-Fe bcc lattice leading to the formation of the bcc α-Fe(Al, Si) disordered solid solution. This structural disorder is commonly obtained in the systems prepared by mechanical alloying as previously mentioned.

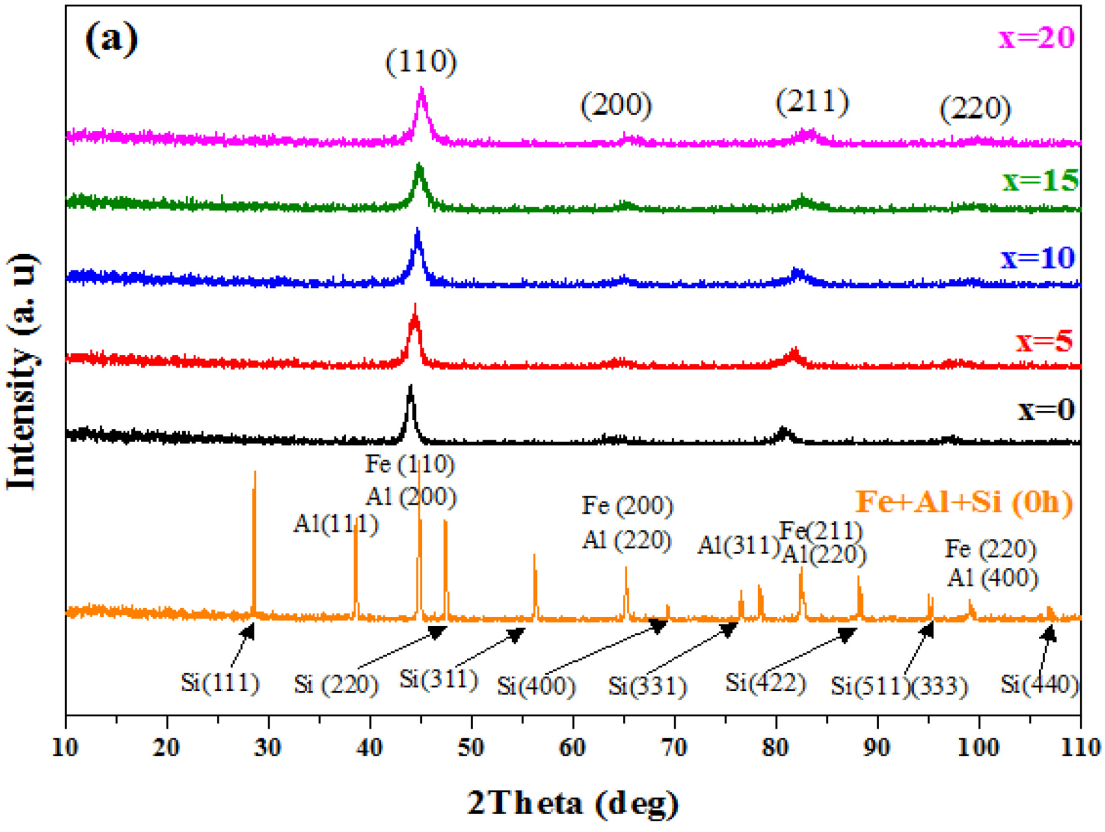

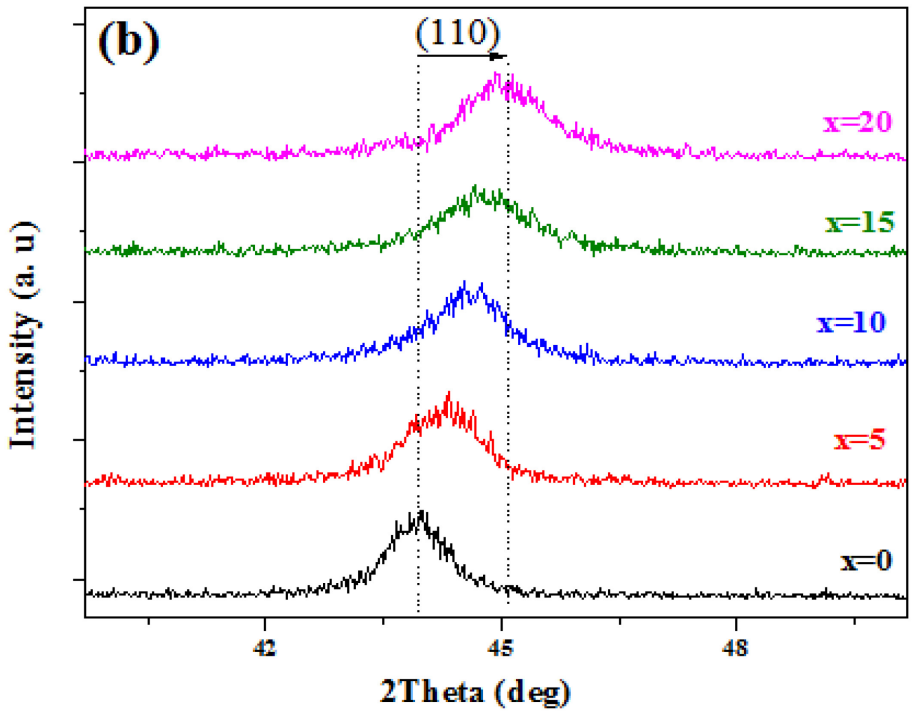

Figure 3. (a) X-ray diffraction patterns of $(Fe_{0.6}Al_{0.4})_{100-x}Si_x$ samples. **(b)** Detail of the most intense Bragg reflection (110).

A rigorous observation of the superposition of the five diffraction patterns shows clearly that the introduction of Si into $Fe_{60}Al_{40}$ alloy produces a shift of the diffraction peaks toward higher angular positions [see Fig. 3b, detail of the most intense Bragg reflection (110)], thus indicating a decrease in the value of the lattice parameter mainly due to the smaller atomic radius of Si compared with those of Fe and Al. We have calculated the values for the lattice parameter, a(Å), from the formula relating to the cubic structure, Eq. (5) [21]:

$$a = d_{hkl}\sqrt{h^2 + k^2 + l^2} \tag{5}$$

were h, k, l are the Miller índices and d_{hkl} is the interplanar spacing.
The obtained results are listed in table 1 and plotted in Fig. 4 where the value for the bcc α-Fe is denoted as a horizontal blue line for comparison. The value of a(Å) is around 2.91 Å for the as-milled binary alloy, in good agreement with that already reported in [22], and it decreases below that corresponding to bcc-Fe, reaching a value of 2.847(2) Å for the alloy with the highest Si content (a decrease of 2.35%). The smaller atomic radius of Si (117 pm) compared with Al (143 pm) and Fe (124 pm) gives rise to a reduction of the lattice parameter value as the Si content increases [8, 9].

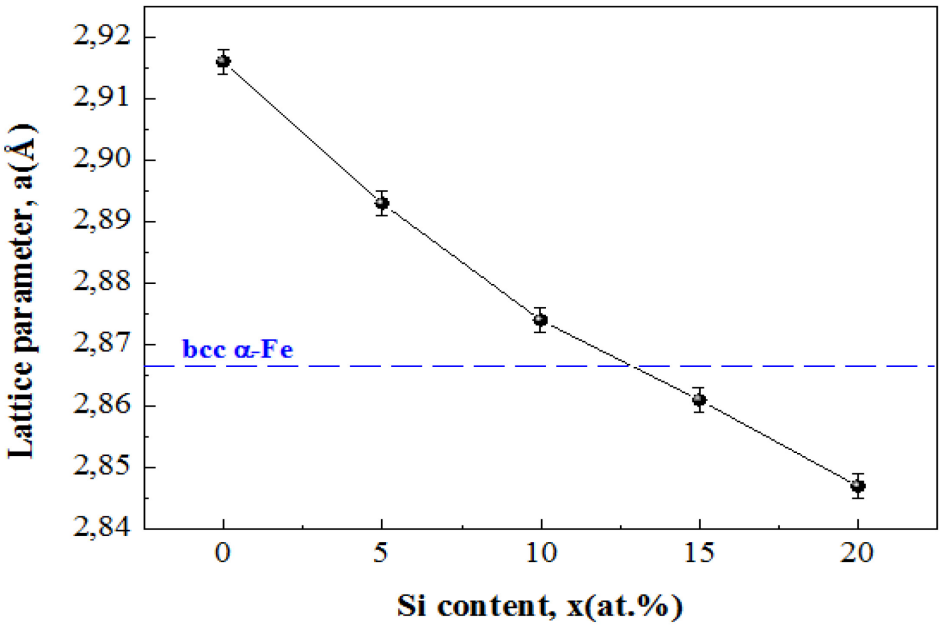

Figure 4. Dependence of lattice parameter with Si content for the $(Fe_{0.6}Al_{0.4})_{100-x}Si_x$powders. The value for bcc-Fe is also included (dotted blue line) for comparison.

Table 1. Estimated values of lattice parameter, a(Å), mean crystallite size, <D(nm)>, volume fraction of grain boundaries, f_{gb}, average level microstrains, **<ε >,** and dislocation density, ρ, of $(Fe_{0.6}Al_{0.4})_{100-x}Si_x$ samples.

Sample	a (Å) ±0.002 Å	<D> (nm) ±1 nm	f_{gb} (%)	<ε > (%)	ρ (10^{16} /m^2)
x=0	2.916	27	10,5(3)	0.85(2)	1.63(8)
x=5	2.890	19	14(7)	1.11(4)	2.8(2)
x=10	2.874	15	18(6)	1.3(3)	4.0(2)
x=15	2.860	10	26(1)	1.54(5)	5.6(4)
x=20	2.847	10	27(1)	1.76(5)	7.0 (4)

Fig. 5 illustrates the evolution of the mean crystallite size, <D> (nm), and the volume fraction of the grain boundaries, fgb (%) as a function of Si content.

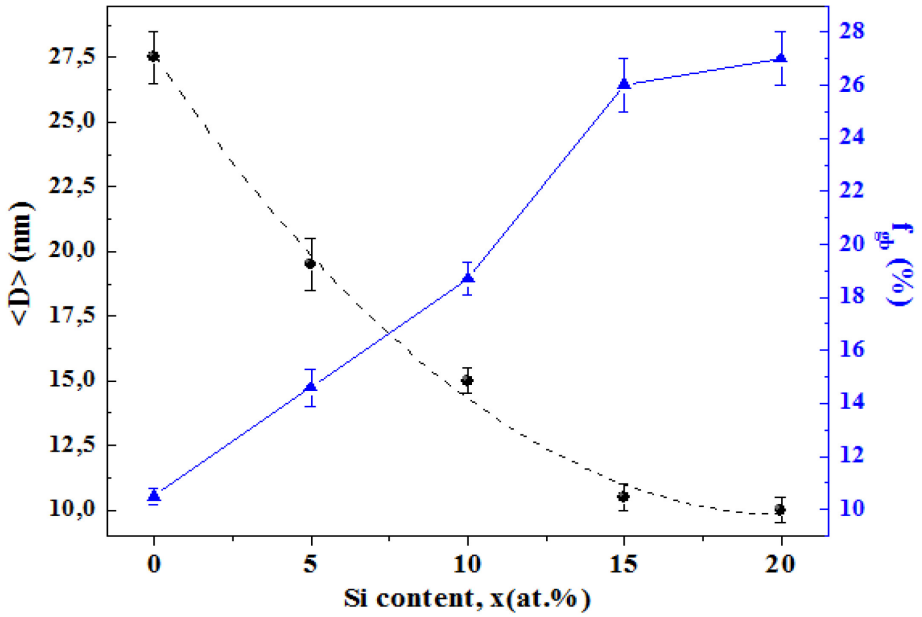

Figure 5. Evolution of mean crystallite size (left y-axis) and volume fraction of the grain boundaries (right y-axis) as a function of Si content. The dotted line represents an exponential fit of the data.

The mean crystal size vs. Si content follows an exponential decrease, and its value falls from about 27 nm for the as-milled binary alloy to 10 nm for the alloys with x>15 (see table 1). As previously mentioned [8, 9, 17, 23], the decrease of <D> is mainly due to the fact that the brittle nature of Si enhances the material hardening and therefore the easy fragmentation of the powders as the amount of Si increases, leading to a diminution of the crystalline size. However, the fact that <D> remains unchanged for x above 10% is probably due to the fact that silicon favours the increase of the local internal strain compared to the reduction in size of the crystallites, hence, regarding the preparation conditions; the limit of Si content which can provokes a clear reduction of the crystallite size may be around 15%. Turning to the analysis of the volume fraction of the grain boundaries, fgb, it shows an opposite trend to that of <D> (see Fig. 5, right y-axis); the addition of silicon provokes the increase of the volume fraction occupied by the grain boundaries (from about 10% to 27% for x=0 and x=20 respectively, see table 1), which is a direct consequence of the grain refinement.

More information about the microstructure of the powders can be obtained by considering the evolution of the average microstrain, <ε > (%), as a function of Si content (see Fig. 6).

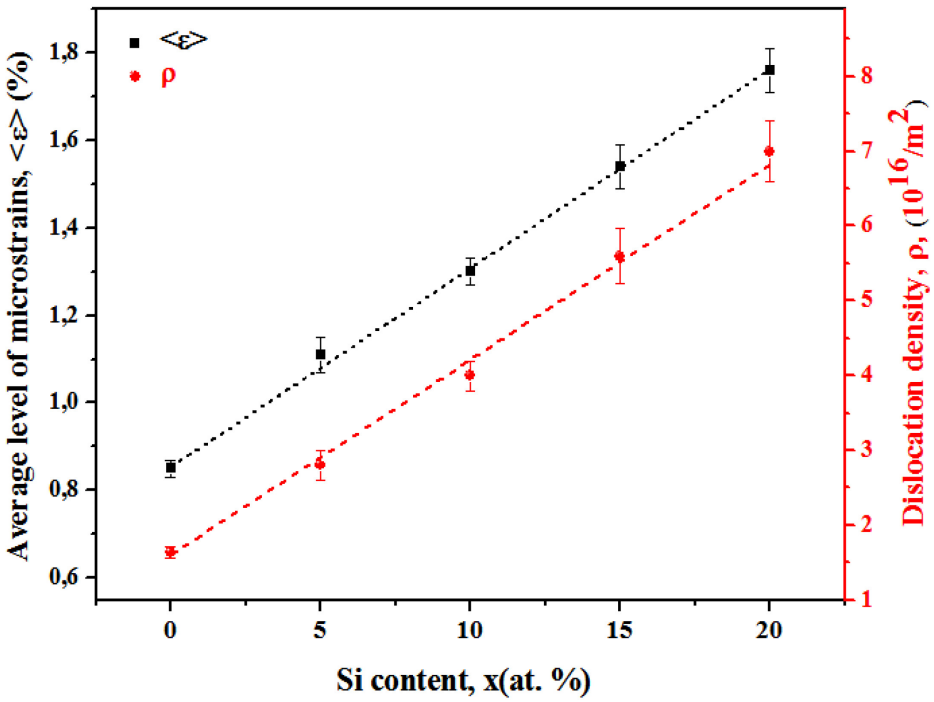

Figure 6. Variation of average microstrain (left y-axis) and the dislocation density (right y-axis) for $(Fe_{0.6}Al_{0.4})_{100-x}Si_x$powders. The dotted line represents a linear fit of the data.

As we could expect, <ε (%)> is higher for the samples enriched in Si and exhibits a linear trend. Its value is double for the sample with the highest silicon content (1.76 (5) %) compared with that for the binary alloy (0.85(2) %). This increase of <ε >, could be due to stress fields associated with the multiplication of dislocations [24, 25].

In order to see the relationship between the microstrain and the dislocations, we have calculated the dislocation density, ρ (m^{-2}) using the following formula [26]:

$$\rho = 14.4\frac{\varepsilon^2}{b^2} \quad (6)$$

where, b is the magnitude of the Burgers vector, ε is the microstrain. The direction of the b vector depends on the plane of dislocation, which is usually on the closest-packed plane of the unit cell. In the case of bcc-Fe, the closest-packed plane is (111). The magnitude of b is given by [27]:

$$b = \frac{a}{2}\sqrt{h^2 + k^2 + l^2} \quad (7)$$

where a is the lattice parameter of the crystal and h, k, and l are the Miller indices.

The calculated values of dislocation density for $(Fe_{0.6}Al_{0.4})_{100-x}Si_x$ powders as a function of Si content are also recorded in table 1 and shown in Fig.6 (see right y-axis). It is clear that ρfollows an almost linear trend, likewise the lattice microstrain does. Hence, the increases of ε and ρ and closely related. Moreover, a higher volume fraction occupied by the grain boundaries could also cause a larger lattice strain.

3.3. Hysteresis curves

The hysteresis loops, M(H), for the all samples are presented in Fig.7 It is clearly seen that with increasing Si content, the magnetization value is reduced.

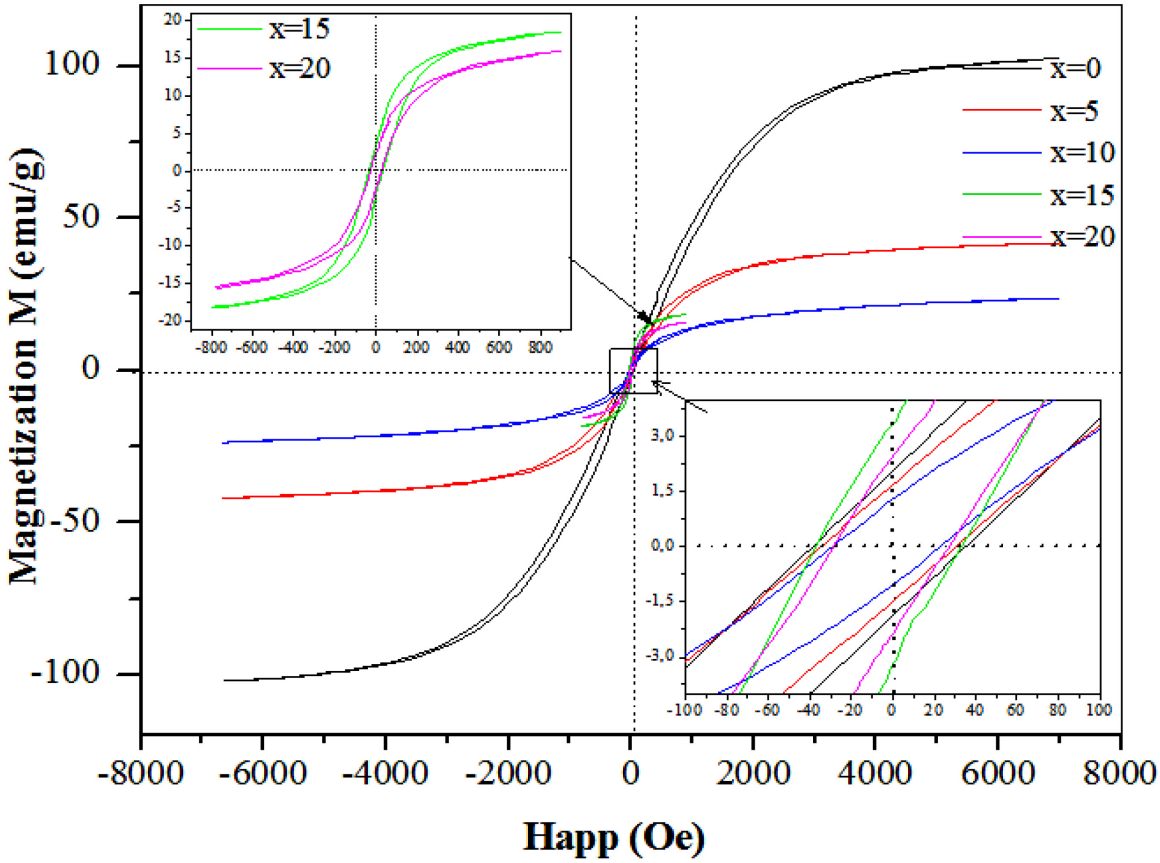

Figure 7. Hysteresis loops for the five $(Fe_{0.6}Al_{0.4})_{100-x}Si_x$samples.

The value of the saturation magnetization, M_S, has been estimated from the high magnetic field region of the M(H) curves using a fit to an approach-to-saturation law [28]:

$$M = M_S\left(1-\frac{a}{H}-\frac{b}{H^2}\right)+\chi H \qquad (8)$$

where *a* is a coefficient related to defects and/or microstress, *b* is a coefficient related to crystal anisotropy and χ is ascribed to an independent field susceptibility.

The obtained values of Ms as a function of Si content are recapitulated in Table 2 and shown on Fig.8. The value of Ms strongly dependson the Si content, it's value is around 102 emu/g for the binary alloy and drastically falls down to 41.5 emu/g for the alloy with x=5% ($Fe_{57}Al_{38}Si_5$). These values are in good agreement with the data reported for the ball-miled $Fe_{60}Al_{40}$ [29] and $Fe_{56}Al_{24}Si_{20}$ [9], respectively. For Si content above 5 at%, a further decrease of the saturation magnetization, but less pronounced, occurs reaching a value of about 15 emu/g for x=20 (see Fig. 8 and Table 2). Moreover, it is interesting to note that, in the present work, the behavior of Ms is similar to that of Fe/Si ratio and<D> (see Fig. 8 and Fig. 5). Under these findings and since the Fe/Al ratio is constant, the decrease of Ms could be mainly due to small variations of the Fe-Fe interatomic distances due to the insertion of smaller Si atoms in the lattice. Furthermore, the silicon decreases the magnetic moment of

individual Fe sites due to a decrease in the direct ferromagnetic interaction between Fe-Fe sites. In order to get a quantitative information about the moment carried by each Fe atom in all the samples, we have estimated the values of magnetic moment per Fe atom (μ_{Fe} in μB/at. Fe) using the formula of the Eq. (9), [30, 31] and taking into account the percentage of Fe atoms in the samples.

$$\mu_B = \frac{M_w \times M_s}{5585} \quad (9)$$

where M_w is the molecular weight of the sample, Ms is the saturation magnetization and 5585 is a magnetic factor. The obtained values of μ_{Fe} for $(Fe_{0.6}Al_{0.4})_{100-x}Si_x$ powders as a function of Si content are also recorded in Table 2 and shown in Fig.8. We see that the evolution of μ_{Fe} vs. Si content follows the same trend as Ms. The decrease of μ_{Fe} with x is consistent with the modification of the density of states at Fermi level. Indeed, it has been reported that when adding Si to Fe-based alloys, and with increasing Si content, more Si atoms ([Ar] $3s^2$ $3p^2$) will be dissolved into the Fe ([Ar] $3d^6 4s^2$) lattice enhancing the electron transfer from 3p Si band to 3d Fe band and resulting in a reduction of the iron magnetic moment μ_{Fe} [8-12].

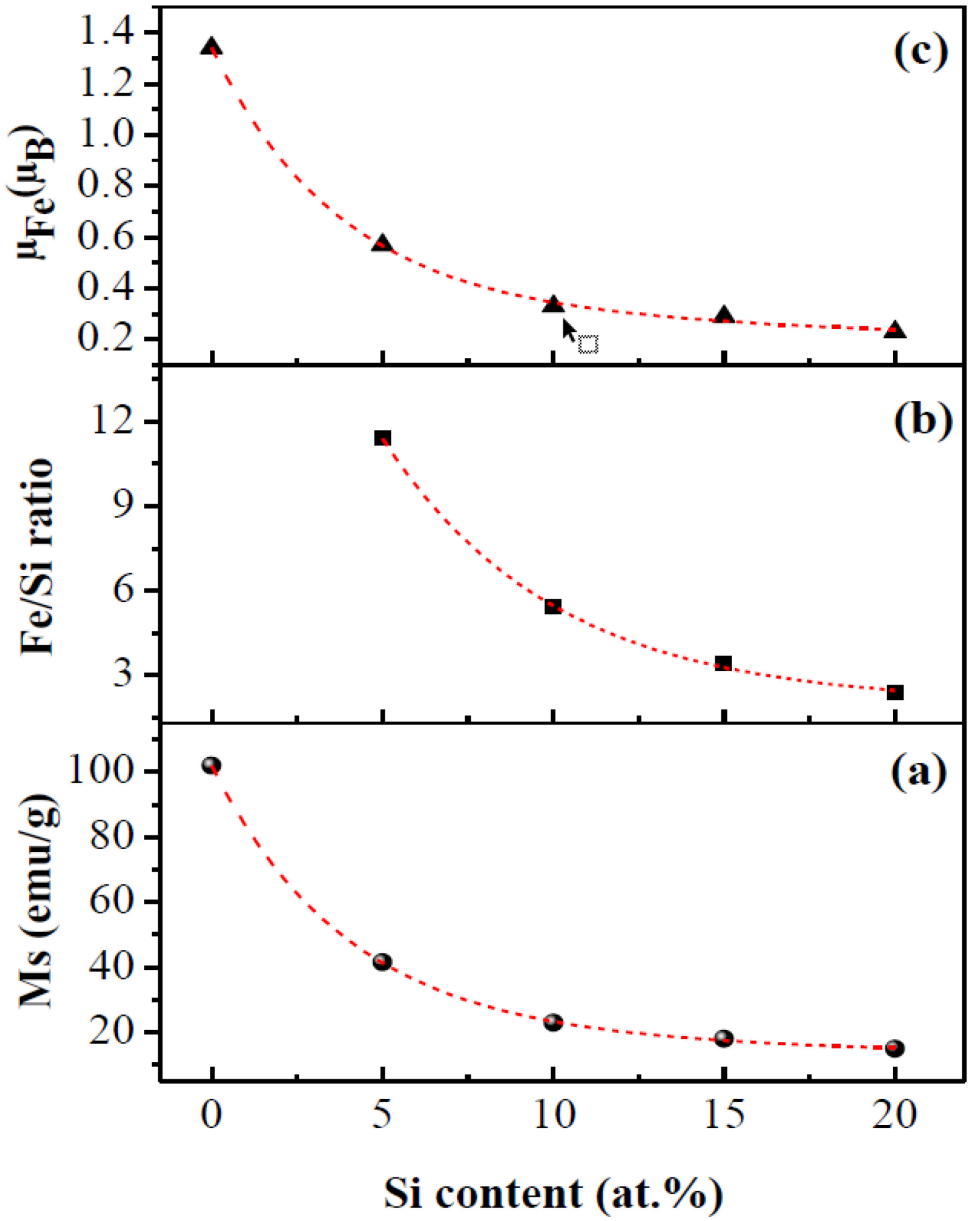

Figure 8. Variation of(a) the saturation magnetization, Ms, (b) the Fe/Si ratio and (c) the magnetic moment per Fe atom, μ_B as a function of Si content.

Table 2. Values of the saturation magnetization, Ms, magnetic moment per Featom, μ_{Fe}, and coercive field, Hc, for the $(Fe_{0.6}Al_{0.4})_{100-x}Si_x$nanostructured powders.

Sample	Ms (emu/g) ± 1emu/g	μ_{Fe} (μ_B)	Hc (Oe)±2 Oe
x=0	102	1.34	40
x=5	40	0.57	30
x=10	23	0.33	25
x=15	18	0.29	30
x=20	15	0. 23	38

Fig. 9, shows the evolution of Hc as a function of Si content and the values are depicted on Table 2. Two stages can be observed on Figure 9: a first stage where Hc decreases from 40 Oe (x=5 at.% Si) to a minimum value of 25 Oe (x=10 at.% Si) and a second stage marked by an increase of Hc reaching a maximum of 38 Oe for 20 at.%Si.

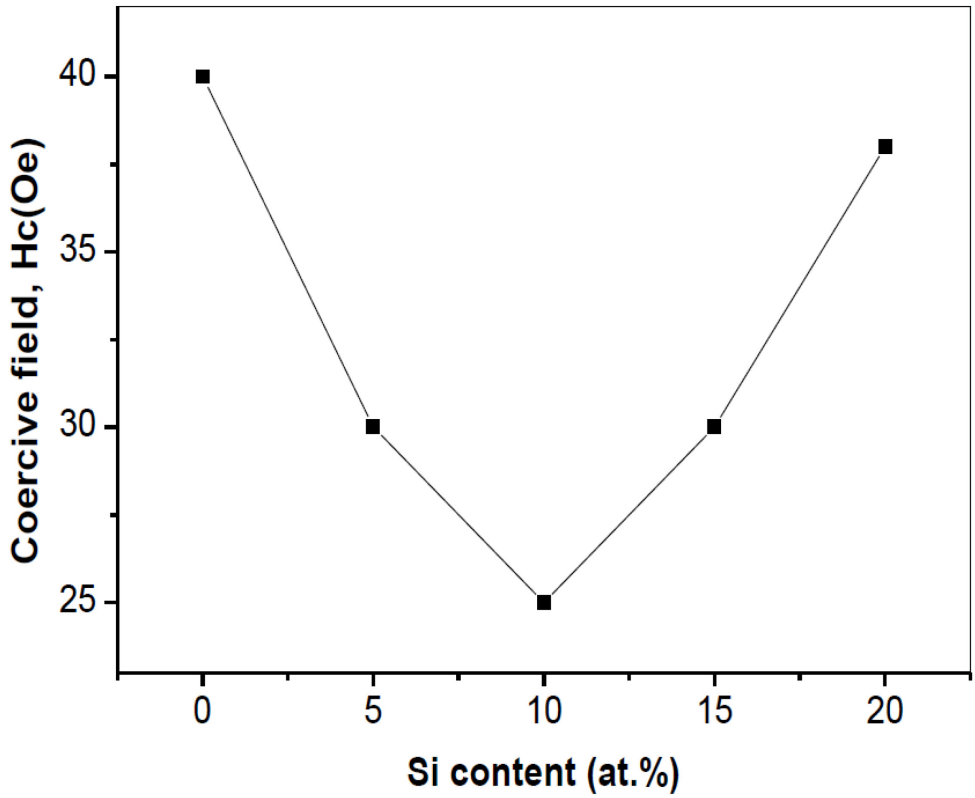

Figure 9. Variation of coercive field as a function of Si content

With reference to random anisotropy model (RAM), when the crystallite size of nanocrystalline materials is less than the exchange correlation length (Lex), the variation of coercivity follows a law in D^6 [4]. In this work, the values of <D(nm)> varied between 19 nm and 10 nm and are lower than the typical value of L_{ex} equal to 23 nm for nanocrystalline Fe-based alloys [32]; hence according to random anisotropy model, this leads to a decrease of Hc. However, the increase of Hc beyond x=10 at.% cannot be explained by the RAM model, despite that <D(nm)> still decreases with increasing Si content. We belive that the increase of Hc could be attributed to the change in GBs due to the non dissolved Si atoms which acts as magnetic inclusions and block the domains walls motion (domain wall anchoring) [9].

3.4. Mössbauer analysis

Fig.10 shows the Mössbauer spectra and their corresponding hyperfine field distributions (HFD).

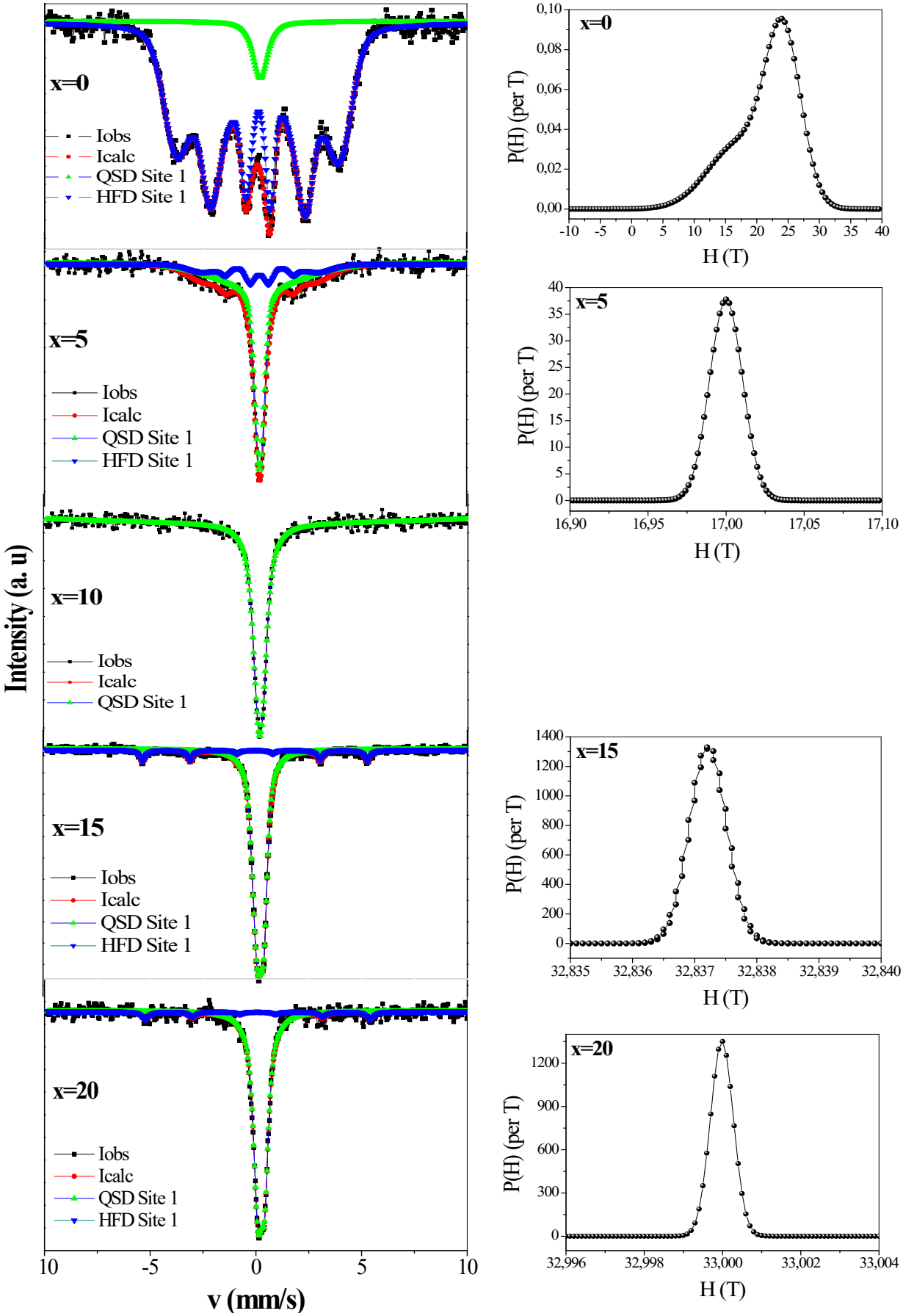

Figure 10. Room temperature Mössbauer spectra and magnetic hyperfine field distributions for the five $(Fe_{0.6}Al_{0.4})_{100-x}Si_x$ powders.

For the as-milled binary alloy (x=0), the spectrum was fitted by considering two main different sites: the first centred paramagnetic singlet (with weak relative area, 4.5%, and mean isomer shift <IS> around 0.2 mm/s) whose origin could be attributed to the formation of an Al-rich α-Fe(Al) phase. The second one, a ferromagnetic contribution (sextet) with spectral lines much broader than those of pure iron (0.12 mm/s) which can be attributed to the formation of a bcc Fe(Al) solid solution with disordered magnetic iron sites that are occupated randomly by Al atoms. The hyperfine field distribution (HFD) corresponding to the sextet contains two regions associated to different environments of iron atoms surrounded by aluminium and silicon atoms: a peak with a maximum around 24 T and a shoulder with a most probable Fe site of 17 T, which correspond to the following atomic configurations in the first (NN) and in the second neighbour (NNN) shells around the Fe atoms: [(5Fe+3Al)NN+(4Fe+2Al)NNN] and [(4Fe+4Al)NN+(0Fe+6Al)NNN], respectively. Note that these configurations were deduced by the application of the local environment model [32-36] after the fit of the spectra, in which the magnetic moment of an element depends on the number of nearest neighbors (NN) (see ref [8] for more details). The first component of 24 T comes from the Fe atoms inside the nanocrystals and corresponds to the Fe-rich α-Fe (Al) phase and the second component (the low Hhf shoulder) can be attributed to a similar phase but less rich in Fe or to Fe atoms localized at grain boundaries [8]. The two components calculated from HFD gives a mean quadratic hyperfine field, <|Hhf|>, of 21T. It is worth noting that the Mössbauer spectrum we have collected for disordered $Fe_{60}Al_{40}$ alloy is completely different from those already reported for the identical composition of alloy, prepared by melting in arc furnace and by induction melting techniques [22, 37]. Indeed, E. Legarra et al. [37] found that the Mössbauer spectrum of ordered binary $Fe_{60}Al_{40}$ alloy shows only paramagnetic contribution (singlet) and the mechanical deformation of this alloy cause the appearance of a weak ferromagnetic contribution (sextet). Also G. A. Peérez Alcázar et al. [22] found that the Mössbauer spectrum corresponding to disordered $Fe_{60}Al_{40}$ is composed of a dominant paramagnetic singlet and a very weak ferromagnetic sextet with a $<|H_{hf}|>$ of around 19 T, contrary to our case where the spectrum is composed of a both dominant sextet and a weak paramagnetic singlet. The authors explained these findings by the fact that the structural disorder in binary Fe-Al alloys reinforces the ferromagnetic exchange due to the larger effective number of magnetic NN in the disordered phase compared with the ordered one.

For the ternary alloys, we have observed a significant change in the shapes of the spectra as more Si atoms are introduced into the lattice. Indeed, the introduction of a low quantity of Si (5 at. %) into the bcc solid solution provokes an increase of the relative area of the singlet to 77.5% and decreases that of sextet to 22.5%, respect to those of the binary $Fe_{60}Al_{40}$ solid solution. As one can see, the sextet can be fitted properly taking into account a single HFD with a mean hyperfine magnetic fiel of 17 T, the same value as that of the shoulder already observed. Increasing Si content to 10 at.%, the ferromagnetic sextet entirely disappears and the spectrum consist only of the paramagnetic contribution (singlet) with an identical isomer shift,<IS>, that found at x=0 and 5 at. % (≈ 0.2 mm/s). The singlet is generally attributed to paramagnetic domains with symmetrical surrounding of Fe by non-ferromagnetic atoms of Si and/or Al, that is domains of the B2 ordered phase [38-41]; however, in the present study, no ordered phase was observed in XRD spectra which showed only the formation of the disordered (bcc) solid solution (see section 3.2). Hence, this single phase corresponds to paramagnetic disordered $Fe_{54}Al_{36}Si_{10}$ solid solution. Finally, the Mössbauer spectra for the samples with higher Si content (x=15 and x=20) are almost identical and were ajusted with two sub-spectra: one is a dominant doublet with a quadrupole splitting, <QS>, around 0.33 mm/s and an isomeric shift <IS> of 0.26 mm/s, is probably due to the formation of a superparamagnetic Fe(Al, Si) solid solution as a consequence of the small size (~10 nm). The other is a minor sextet with narrow lines and an HFD which have the shape of a simple Gaussian function centered on ~33 T. This component corresponds to atomic configurations with (8Fe in NN + 6Fe in NNN) and may be due to the formation of Fe clusters in these alloys [42].

4. Summary and Conclusion

Single phase nanocrystalline Fe(Al, Si) solid solutions have been successfully fabricated, from the mixture of elemental Fe, Al and Si powders, by high energy mechanical alloying process for a milling time of 72 h. The XRD profiles analysis have shown that the obtained Fe(Al, Si) alloys are single phase in the whole range of Si content and exhibit a disordered bcc crystal structure with a lattice parameter which decreases as the Si content increases. The insertion of Si atoms into the α-Fe lattice leads to a progressive diminution of the mean crystallite size and a linear increase of the average microstrain and the dislocation density. The SEM images suggest that the addition of Si stimulate the reduction of the powder particle size. Mössbauer spectroscopy corroborates the formation of Fe (Al, Si) solid solution as concluded from XRD spectra and also provided additional details on the differences in the local environments of the Fe atoms in the disordered Fe(Al, Si) phase with different amount of Fe, Al and Si but having the same bcc lattice. These details, which cannot be revealed neither by X-ray diffraction nor by magnetization measurements, allows for a clear understanding of the relationship between the structure and microstructure of disordered Fe(Al, Si) alloys and the corresponding hyperfine and magnetic properties.

References

[1] A. Hajalilou, A. Kianvash, H. Lavvafi, K. Shameli, Nanostructured soft magnetic materials synthesized via mechanical alloying: a review, J Mater Sci: Mater Electron, Journal of Materials Science: Materials in Electronics, 29(2), (2017) 1690–1717.

[2] F. Hadef, A. Otmani, Mechanical Alloying/Millin,. Handbook of Mechanical Nanostructuring, (2015), 263-276

[3] C. Suryanarayana, Mechanical alloying and milling, Prog. Mater. Sci. 46 (2001) 1-184.

[4] G. Herzer, Nanocrystalline soft magnetic materials, J. Magn. Magn. Mater. 157/158 (1996) 133-136.

[5] F. Hadef, Solid-state reactions during mechanical alloying of ternary Fe-Al-X (X=Ni, Mn, Cu, Ti, Cr, B, Si) systems: A review, J. Magn. Magn. Mater. 419 (2016) 105-118.

[6] G. A. Pérez Alcázar, L. E. Zamora, J. D. Betancur-Ríos, J. A. Tabares, J. M. Greneche, J. M. González, Effect of Si on the magnetic properties of the $Fe_{70}Al_{30}$ alloy, Physica B. 384 (2006) 313-315.

[7] G. Y. Vélez, G. A. Pérez Alcázar, L. E. Zamora, J. J. Romero, A. Martìnez, Infuence of silicon and atomic order on the magnetic properties of $(Fe_{80}Al_{20})_{100-x}Si_x$ nanostructured system, J. Hyper. Inter. 195 (2010) 179-184.

[8] N. Boukherroub, A. Guittoum, A. Laggoun, M. Hemmous, D. Martínez-Blanco, J. A. Blanco, N. Souami, P. Gorria, A. Bourzami, O. Lenoble, Microstructure and magnetic properties of nanostructured $(Fe_{0.8}Al_{0.2})_{100-x}Si_x$ alloy produced by mechanical alloying, J. Magn. Magn. Mater. 385 (2015) 151-159.

[9] M. Hemmous, A. Guittoum, M. Kezrane, N. Boukherroub, D. Martínez-Blanco, P. Gorria, J. A. Blanco, N. Souami, N. Fenineche, Effect of Si addition on the structural, microstructural and magnetic properties of $(Fe_{70}Al_{30})_{100-x}Si_x$ nanostructured powders elaborated by mechanical alloying, J. Magn. Magn. Mater. 439 (2017) 188-195.

[10] R. Bernal-Correa, A. Rosales-Rivera, P. Pineda-Gomez and N. A. Salazar, J. Alloys Comp.495, 491 (2010).

[11] Y. Jiraskova, J. Bursik, J. Cizek and D. Jancik, J. Alloys Comp. 568, 106 (2013).

[12] High Score software for crystallography, Philips analytical, 2002.

[13] G. K. Williamson and W. H. Hall, X-ray line broadening from filed aluminium and wolfram, Acta Metal. 1 (1953) 22-31.

[14] M. Yousefi, S. Sharafi,The effect of simultaneous addition of Si and Co on microstructure and magnetic properties of nanostructured iron prepared by mechanical alloying, Mater. Design 37 (2012) 325-333.

[15] E. Jartych, Local atomic order in nanocrystalline Fe-based alloys obtained by mechanical alloying, J. Magn. Magn. Mater. 265 (2003) 176-188.

[16] K. Lagarek, D. Rancourt, Recoil Software, Physics Department, University of Ottawa, 1998.

[17] M. Hocine, A. Guittoum, M. Hemmous, D. Martínez-Blanco, P. Gorria, B. Rahal, J. A. Blanco, J. J. Sunol, A. Laggoun, The role of silicon on the microstructure and magnetic behaviour of nanostructured $(Fe_{0.7}Co_{0.3})_{100x}Si_x$ powders, J. Magn. Magn. Mater. 422 (2017) 149-156.

[18] JCPDS card N° 00-006-0696.

[19] JCPDS card N° 00-001-1176.

[20] JCPDS card N° 00-027-1402.

[21] A. Clearfield, J. Reibenspies and N. Bhuvanesh, Principles and Applications of Powder Diffraction, 2008 Blackwell Publishing Ltd. ISBN: 978-1-405-16222-7.

[22] G. A. Peérez Alcázar and Galvão da Silva, Mossbauer effect study of magnetic properties of $Fe_{1-q}Al_q$, $0 < q < 0.5$, alloys in the disordered phase**,** J. Phys. F: Met. Phys. 17(1987) 2323-2335.

[23] M. Hemmous and A. Guittoum, Elaboration, structure and Mössbauer spectroscopy of nanostructred Fe_{100-x} Si_x powders elaborated by mechanical alloying, SPIN 7 (2017) 1-8.

[24] A. Sharifati, S. Sharafi, Structural and magnetic properties of nanostructured $(Fe_{70}Co_{30})_{100x}Cu_x$ alloy prepared by high energy ball milling, Mater. Desig 41 (2012) 8-15.

[25] A. K. Singh, Advanced X-ray techniques in research and industry, IOS press, 2005.

[26] S. Takebayashi, T. Kunieda, N. Yoshinaga, K. Ushioda and S. Ogata, Comparison of the dislocation density in martensitic steels evaluated by some X-ray diffractionmethods, ISIJ International, 50 (2010) 875-882.

[27] H. Laala-Bouali, F.Z. Bentayeb, S. Louidi, X. Guo, S. Tria, J. J. Suñol, L. Escoda, X-ray line profile analysis of the ball-milled Fe–30Co alloy, Advan. Powd. Techno. 24 (2013) 168-174.

[28] B. D. Cullity, C.D. Graham, Introduction to Magnetic Materials, John Wiley and Sons, Inc., Hoboken, New Jersey, 2009.

[29] S. Gialanella, X. Amils, M. D. Barò, p. Delcroix, G. Le Caër, L. Lutterotti and S. Suriñach, Microstructural and kinetic aspects of the transformations induced in a feal alloy by ball-milling and thermal treatments, Acta mater. 46 (1998) 3305-3316.

[30] M. Satalkar, N. Ghodke, S. N. Kane, Influence of high temperature sintering on the structural and magnetic Properties of $Mn_{1-x}Zn_xFe_2O_4$, J. Phys: Conference Series. 534 (2014) 012016

[31] K. Rama Krishna, K. Vijaya Kumar, C. Ravindernathgupta, Dachepalli Ravinder, Magnetic properties of Ni-Zn ferrites by citrate gel method, Advan. Mater. Phys. Chemi. 2 (2012) 149-154.

[32] M.B. Stearns, Variation of the internal fields and isomer shifts at the Fe sites in the FeAl series, J. Appl. Phys. 35 (1964) 1095-1096.

[33] G. K. Wertheim, V. Jaccarino, J. H. Wernick, D.N.E. Buchanan, Range of the exchange interaction in iron alloys, Phys. Rev. Lett. 12 (1964) 24-27.

[34] E. Jartych, Local atomic order in nanocrystalline Fe-based alloys obtained by mechanical alloying, J. Magn. Magn. Mater. 265 (2003) 176-188.

[35] M. B. Stearns, Internal magnetic fields, isomer shifts, and relative abundances of the various Fe sites in FeSi Alloys, Phys. Rev. 129 (1963) 1136-1144.

[36] S. M. Dubiel, W. Zinn, Influence of Si on spin and charge density changes in bcc-Iron, J. Magn. Magn. Mater. 28 (1982) 261-276.

[37] E. Legarra, E. Apinaniz, F. Plazaola, Mösbauer spectroscopy study of the influence of Si addition to ordered and disordered $Fe_{60}Al_{40}$ alloys,J. Phys.: Conference Series. 217(2010) 012078.

[38] L. M. Kubalova, I. A. Sviridov, O.Ya Vasilyeva, V. I. Fadeeva, Structural transformation in mechanosynthesized bcc Fe-Al-Si(Ge) solid solutions during heating, J. Alloys. Compd. 434–435 (2007) 467-471.

[39] A. Hanc, J. Kansy, G. Dercz, I. Jendrzejewska, Point defect structure in B2-ordered Fe-Al alloys, J. Alloys Compd. 480 (2009) 84-86.

[40] M. Krasnowski, A. Grabias, T. Kulik, Phase transformations during mechanical alloying of Fe-50% Al and subsequent heating of the milling product, J. Alloys Compd. 424 (2006) 119-127.

[41] Varkey Sebastian, N. Lakshmi, Snehal Jani, K. Venugopalan, Magnetic properties of nano-sized 5 at.%Fe-Al systems, J. Nano. Res. 13 (2011) 5627-5633

[42] N. Boukherroub, A. Guittoum, N. Souami, K. Akkouche, S. Boutarfaia, Structural, microstructural and Mössbauer studies of nanocrystalline Fe_{100-x} Al_x, powders elaborated by mechanical alloying, Eur. Phys. J. Web Conf. 29 (00010) (2012) 1-7.